

# Isomer-Specific Fuel Destruction Pathways in Rich Flames of Methyl Acetate and Ethyl Formate and Consequences for the Combustion Chemistry of Esters<sup>†</sup>

Patrick Osswald,<sup>‡</sup> Ulf Struckmeier,<sup>‡</sup> Tina Kasper,<sup>‡</sup> Katharina Kohse-Höinghaus,<sup>\*,‡</sup>  
Juan Wang,<sup>§</sup> Terrill A. Cool,<sup>\*,§</sup> Nils Hansen,<sup>⊥</sup> and Phillip R. Westmoreland<sup>||</sup>

Department of Chemistry, Bielefeld University, Universitätsstrasse 25, D-33615 Bielefeld, Germany, School of Applied and Engineering Physics, Cornell University, Ithaca, New York 14853, Combustion Research Facility, Sandia National Laboratories, Livermore, California 94551, and Department of Chemical Engineering, University of Massachusetts, Amherst, Massachusetts 01003

Received: December 5, 2006; In Final Form: February 6, 2007

The influences of fuel-specific destruction pathways on flame chemistry are determined for two isomeric ester fuels, methyl acetate,  $\text{CH}_3(\text{CO})\text{OCH}_3$ , and ethyl formate,  $\text{H}(\text{CO})\text{OC}_2\text{H}_5$ , used as model representatives for biodiesel compounds, and their potential for forming air pollutants is addressed. Measurements are presented of major and intermediate species mole fractions in premixed, laminar flat flames using molecular-beam sampling and isomer-selective VUV-photoionization mass spectrometry. The observed intermediate species concentrations depend crucially on decomposition of the different radicals formed initially from the fuels. The methyl acetate structure leads to preferential formation of formaldehyde, while the ethyl formate isomer favors the production of acetaldehyde. Ethyl formate also yields higher concentrations of the  $\text{C}_2$  species ( $\text{C}_2\text{H}_2$  and  $\text{C}_2\text{H}_4$ ) and  $\text{C}_4$  species ( $\text{C}_4\text{H}_2$  and  $\text{C}_4\text{H}_4$ ). Benzene concentrations, while larger for ethyl formate, are at least an order of magnitude smaller for both flames than seen for simple hydrocarbon fuels (ethylene, ethane, propene, and propane).

## 1. Introduction

Interest is growing in the use of biofuels to reduce the current dependence on conventional fuels derived from petroleum, and to alleviate the harmful effects of global climate change by controlling aerosol formation and decreasing net  $\text{CO}_2$  emissions.<sup>1–3</sup> However, the combustion chemistry of bioderived fuels is not nearly as well documented as that of hydrocarbon fuels. Accurate information on the fuel decomposition and oxidation mechanisms of several classes of oxygenated fuels including alcohols, ethers, and esters are urgently needed to characterize their potential vehicle emission characteristics, which are of paramount significance in the control of airborne toxics. Also needed is a mechanistic characterization of the role of the oxygenate function in reducing the formation of carbon monoxide, unburned hydrocarbons, polycyclic aromatic species, and soot on the one hand and the increase in  $\text{NO}_x$  emission and undesired oxygenated pollutant species such as aldehydes and ketones on the other. Several classes of constituents, including carbonaceous aerosols and oxygenated species derived from biofuel combustion, can cause important and potentially harmful climatic effects.<sup>2,4</sup> Rigorous analysis and fundamental understanding of principal chemical reaction networks are thus prerequisites for mitigating unwanted emissions. Experimental determinations of the composition of the intermediate species pool formed by combustion reactions are vital to the development of appropriate chemical models.<sup>5</sup>

Biodiesel fuels typically contain monoalkyl, often methyl and ethyl, esters of long-chain fatty acids, derived from vegetable oils or animal fats. Detailed reaction mechanisms for the combustion of esters are largely lacking, despite their importance as biodiesel constituents. In general, combustion performance is influenced by the chemical nature of the esters in the biodiesel fuel and their structural features, including the length of the alkyl chain and their degree of saturation and branching.<sup>6–8</sup> Some early studies have addressed the pyrolysis and reaction kinetics of alkyl esters, including methyl acetate, ethyl acetate, methyl propionate, isopropyl acetate, and ethyl formate.<sup>9–12</sup> Additional attention has been devoted to characterizing the oxidation pathways of esters in the atmosphere.<sup>13,14</sup> More recently, the combustion chemistry of esters has attracted renewed attention, and experimental details on the oxidation and combustion kinetics of methyl acetate, methyl formate, methyl butanoate,  $\text{C}_4$  fatty acid methyl esters, and rapeseed oil methyl ester have been reported.<sup>15–19</sup>

The accurate description of the chemical kinetic reaction mechanisms responsible for observed changes in the composition of combustion byproducts<sup>20,21</sup> when biodiesel is used as a replacement for, or additive with, conventional diesel fuel presents a significant scientific challenge. Some recent modeling studies,<sup>5,15</sup> relying in part on early experimental data,<sup>22–24</sup> emphasize the need for detailed measurements with modern methods of a large number of species under different combustion conditions. Molecular-beam mass spectrometry is ideally suited for this task. The use of easily tunable VUV synchrotron radiation with a time-of-flight mass analyzer permits simultaneous measurements of the complete mass range of sampled flame gases with isomeric selectivity.<sup>25,26</sup>

To study the predominant chemical reactions in the degradation and oxidation of ester fuels, we have focused on measure-

<sup>†</sup> Part of the special issue "James A. Miller Festschrift".

\* Corresponding authors. E-mail: (K.K.-H.) kkh@pc1.uni-bielefeld.de; (T.A.C.) tac13@cornell.edu.

<sup>‡</sup> Department of Chemistry, Bielefeld University.

<sup>§</sup> School of Applied and Engineering Physics, Cornell University.

<sup>⊥</sup> Combustion Research Facility, Sandia National Laboratories.

<sup>||</sup> Department of Chemical Engineering, University of Massachusetts, Amherst.

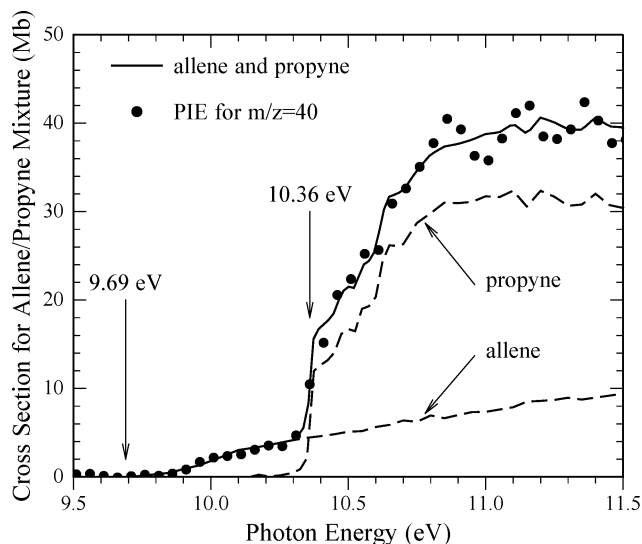


**Figure 1.** Photoionization efficiency (symbols) for  $m/z = 40$  measured for the methyl acetate flame 4.8 mm from the burner. The PIE data have been scaled vertically to match the mean photoionization cross section (solid curve) calculated for an allene/propyne (27%/73%) mixture, chosen to give a best fit to the scaled PIE. The allene and propyne cross sections, weighted by the respective mole fractions, are shown as dashed lines. The respective ionization energies (9.69 and 10.36 eV<sup>35</sup>) of allene and propyne are indicated by the vertical arrows.

ments with photoionization mass spectrometry (PIMS) of species mole fractions in premixed laminar flames fueled by methyl acetate,  $\text{CH}_3(\text{CO})\text{OCH}_3$ , and ethyl formate,  $\text{H}(\text{CO})\text{OC}_2\text{H}_5$ . Semivolatiles practical biodiesel fuel constituents are difficult to study in premixed laminar flames. We have instead chosen to investigate methyl acetate and ethyl formate because they are the smallest pair of structural isomers that allows detailed analysis of the influence of ester functional groups on the fuel consumption pathways. They present an ideal combination with similar overall combustion characteristics (e.g., temperature profiles and exhaust gas composition), which assists quantitative analysis of flame chemistry. Differences in initial fuel destruction reactions and a comparison of the composition of reaction intermediates highlight the influence of fuel structure on the kinetic mechanism, based on the quantitative analysis of 27 flame species.

## 2. Experimental Section

A flame-sampling molecular-beam mass spectrometer employing tunable vacuum-ultraviolet synchrotron radiation for photoionization<sup>25–30</sup> was used to study premixed, low-pressure, flat flames of both esters with identical reagent mole fractions and pressure. Detailed descriptions of the instrument and experimental procedures have been given previously.<sup>26,27,29,30</sup> It consists of a low-pressure flame chamber, a differentially pumped molecular-beam flame-sampling system, and a linear time-of-flight mass spectrometer (TOFMS). It is coupled to a 3-m monochromator used to disperse synchrotron radiation at the Advanced Light Source (ALS) of the Lawrence Berkeley National Laboratory. The monochromator delivers a dispersed photon beam, tunable over the range from 8 to 17 eV, with an energy resolution of 40 meV (fwhm) for the present experiments and a typical photon current of  $5 \times 10^{13}$  photons/s. A silicon photodiode, with its quantum efficiency (electrons/photon) calibrated at the National Institute of Standards and Technology (NIST), records the variation in photon current (photons/s) with photon energy and time.

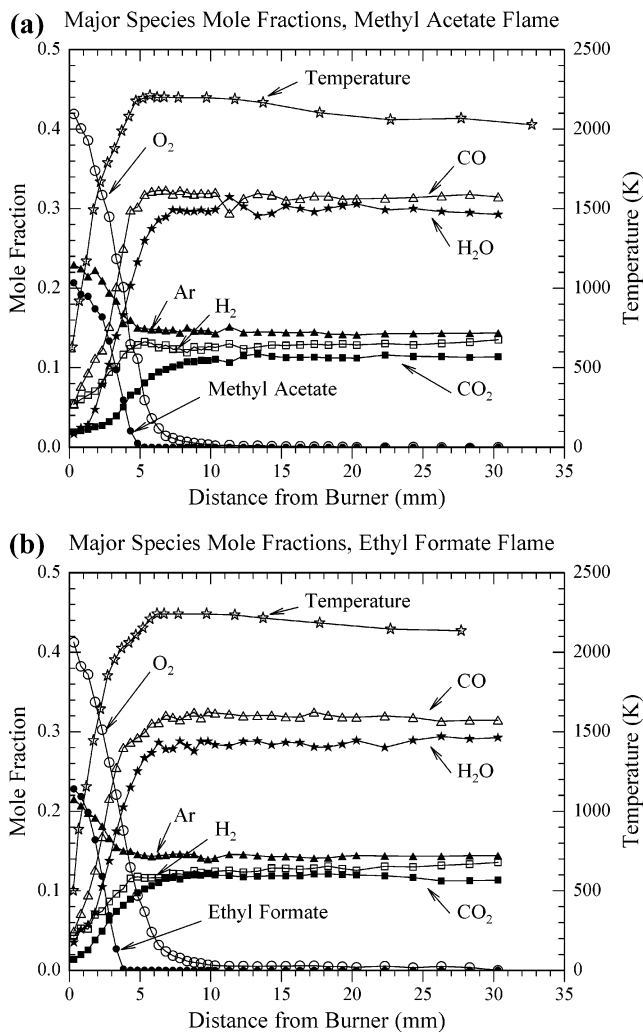


**Figure 2.** Major species mole fractions and flame temperature profiles measured for the methyl acetate (a) and ethyl formate (b) flames.

Premixed fuel/oxygen/argon flames are stabilized on a 6 cm-diameter McKenna burner (Holthuis and Associates). Species mole fractions were measured for premixed  $\text{CH}_3(\text{CO})\text{OCH}_3/\text{O}_2/\text{Ar}$  and  $\text{H}(\text{CO})\text{OC}_2\text{H}_5/\text{O}_2/\text{Ar}$  flames of 25.5%/48.9%/25.6% molar composition and identical equivalence ratio ( $\Phi = 1.82$ ), C/O ratio (0.51), pressure (30.0 Torr), and cold (300 K) flow velocity (64 cm/s). Flame gases are sampled by a quartz cone (Allen Scientific Glass) with a tip of  $40^\circ$  and 0.2 mm orifice diameter located on the flow axis of the flat flame burner. Translation of the burner toward or away from the quartz sampling cone allows mass spectra to be taken at any desired position within the flame. A skimmer of 2.0 mm-diameter aperture placed 23 mm downstream on the axis of the expanded ( $10^{-4}$  Torr) jet forms a molecular beam that passes into the differentially pumped ( $10^{-6}$  Torr) ionization region, where it is crossed by the dispersed VUV light from the monochromator. Photoions are extracted using a pulsed-field technique and mass-analyzed with a 1.3 m linear (Wiley–McLaren)<sup>31</sup> time-of-flight mass spectrometer with a mass resolution  $m/\Delta m = 400$ .

A multichannel scaler (Fast ComTec P7886) records ion counts for a 30  $\mu\text{s}$  sweep (15008 channels of 2 ns bin width) following each gate pulse. Useful mass spectra, with a dynamic range of  $10^5$  are recorded with  $5 \times 10^5$  to  $2 \times 10^6$  sweeps. The ion signal at a given mass/charge ( $m/z$ ) ratio is obtained by integration of the accumulated ion counts per channel over 25 to 40 multiscaler channels (50–80 ns) centered at the mass peak. The total ion count is corrected for the baseline contribution

**TABLE 1: Photoionization Cross Sections  $\sigma(E)$  and Mass Discrimination Factors  $D(M)$** 

$M$	species	cross sections $\sigma(E)^j$	$D(M)$
15	CH <sub>3</sub> <sup>a</sup>	7.6(10.4); 8(11.1)	0.50
16	CH <sub>4</sub> <sup>b</sup>	6.5(13.2)	0.52
18	H <sub>2</sub> O <sup>c</sup>	7.75(13.2)	0.57
26	C <sub>2</sub> H <sub>2</sub> <sup>d</sup>	18.3(11.5); 29.4(12.3); 39(13.2)	0.73
28	C <sub>2</sub> H <sub>4</sub> <sup>d</sup>	8.3(11.1); 8(11.5); 12(12.3)	0.76
29	HCO <sup>e</sup>	5(10.4); 5 (11.1)	0.78
30	CH <sub>2</sub> O <sup>f</sup>	9.2(11.1); 10.2(11.5); 15(12.3)	0.80
32	CH <sub>3</sub> OH <sup>d</sup>	5.8(11.1)	0.83
39	C <sub>3</sub> H <sub>3</sub> <sup>g</sup>	8.8(10.4)	0.93
40	C <sub>3</sub> H <sub>4</sub> (propyne) <sup>d</sup>	17.4(10.4)	0.94
42	CH <sub>2</sub> CO <sup>e</sup>	11(10.4); 12.8(11.1)	0.97
43	CH <sub>3</sub> CO <sup>e</sup>	6(9.65); 6(10.4)	0.98
44	CH <sub>3</sub> CHO <sup>h</sup>	7(10.4); 8.7(11.1)	0.99
46	(CH <sub>3</sub> ) <sub>2</sub> O <sup>d</sup>	7.6(10.4)	1.00
50	C <sub>4</sub> H <sub>2</sub> <sup>d</sup>	17.6(10.4); 28(11.1); 34(11.5); 45(12.3)	1.03
52	C <sub>4</sub> H <sub>4</sub> <sup>d</sup>	11.4(9.65); 30(10.4); 39(11.1); 40(11.5); 42(12.3)	1.04
54	C <sub>4</sub> H <sub>6</sub> <sup>d</sup>	8.2(10.4)	1.05
56	C <sub>4</sub> H <sub>8</sub> /CH <sub>3</sub> CHCO <sup>e</sup>	10.6(10.4)	1.06
58	(CH <sub>3</sub> ) <sub>2</sub> CO <sup>d</sup>	11.2(10.4)	1.06
60	CH <sub>3</sub> COOH <sup>e</sup>	10(11.1)	1.07
66	C <sub>5</sub> H <sub>6</sub> <sup>e</sup>	20(10.4)	1.08
74	H(CO)OC <sub>2</sub> H <sub>5</sub> <sup>i</sup>	6(11.1)	1.09
	<i>i</i>	fragment ion ( $m/z = 30$ ): 0.13(11.1)	1.09
	<i>i</i>	fragment ion ( $m/z = 28$ ): 1.05(11.1)	1.09
	<i>i</i>	fragment ion ( $m/z = 28$ ): 9.2(11.5)	1.09
74	CH <sub>3</sub> (CO)OCH <sub>3</sub> <sup>h</sup>	12.2(11.1)	1.09
78	C <sub>6</sub> H <sub>6</sub> <sup>d</sup>	28.3(10.4)	1.09

<sup>a</sup> Taatjes, C. A. Unpublished measurements <sup>b</sup> Samson, J. A. R.; Haddad, G. N.; Masuoka, T.; Pareek, P. N.; Kilcoyne, D. A. L. *J. Chem. Phys.* **1989**, *90*, 6925. <sup>c</sup> Katayama, D. H.; Shaw, Huffman, R. E.; O'Brian, C. L. *J. Chem. Phys.* **1973**, *59*, 4309. <sup>d</sup> Cool, T. A.; Wang, J.; Nakajima, K., Taatjes, C. A.; McIlroy, A. *Int. J. Mass Spectrom.* **2005**, *247*, 18. <sup>e</sup> Estimated. <sup>f</sup> Cooper, G.; Anderson, J. E.; Brion, C. E. *Chem. Phys.* **1996**, *209*, 61. Wang, J., Cool, T. A. Unpublished photoionization efficiency measurements. <sup>g</sup> Robinson, J. C.; Sveum, N. E.; Neumark, D. M. *J. Chem. Phys.* **2003**, *119*, 5311. <sup>h</sup> Person, J. C.; Nicole, P. P. Argonne National Laboratory Radiological Physics Division Annual Report, July 1969-June 1970, ANL7760; Argonne National Laboratory: Argonne, IL, 1970; pp 97. <sup>i</sup> Wang, J.; Cool, T. A. Unpublished measurements. <sup>j</sup> Cross sections  $\sigma$  in Mb ( $10^{-18}$  cm<sup>2</sup>); photon energies  $E$  in eV.

obtained between peaks and the contributions of <sup>13</sup>C isotopomers, and finally normalized by the photon current.

Flame temperatures were measured in separate experiments conducted at Bielefeld University using laser-induced fluorescence (LIF) of seeded NO (0.5%), as described elsewhere.<sup>32</sup> The LIF signal was recorded after excitation of the A–X (0,0) band near 225 nm under reference flame conditions unperturbed by the cone. In this paper the “distance from the burner” is taken to be 0.9 mm (4.5 sampling orifice diameters) less than the actual separation between the burner and the tip of the sampling cone to account approximately for probe sampling effects.<sup>33,34</sup>

**2.1. Species Identifications.** The ALS flame instrument is capable of resolving and identifying isomers and other flame species of near equal masses with ionization thresholds that differ by as little as 100 meV. Measurements of the photoionization signal as a function of the photon energy (photoionization efficiency or PIE) for species of a given  $m/z$  ratio, facilitated by easily tunable monochromated VUV synchrotron radiation, is a valuable tool for determinations of the isomeric composition of combustion intermediates.<sup>25</sup>

A PIE curve recorded for  $m/z = 40$  in the methyl acetate flame, displayed in Figure 1, exemplifies the determination of species identities and relative concentrations. The photoion signal at  $m/z = 40$  has been vertically scaled to match the mean photoionization cross section (solid curve) for a mixture of allene/propyne with a best-fit  $27 \pm 3\%/73 \pm 3\%$  isomeric composition, constructed with known photoionization cross sections for allene and propyne.<sup>25</sup> Their respective contributions, weighted by their mole fractions, are given as the dashed curves of Figure 1. The respective ionization energies of 9.69 and 10.36 eV for allene and propyne<sup>35</sup> are indicated by the vertical arrows; their cross sections were determined independently from the

flame measurements in a cold gas flow with reference to the propene cross section.<sup>36</sup>

PIE curves for  $m/z = 44$  were used to determine the relative mole fractions of ethenol, CH<sub>2</sub>CHOH, and acetaldehyde, CH<sub>3</sub>CHO, for both flames, following previous observations in flames of different fuels.<sup>25,37</sup> For ethyl formate, the  $m/z = 44$  mole fraction profile (measured at 11.1 eV) is almost exclusively acetaldehyde, while for methyl acetate, the  $m/z = 44$  PIE curve is noisy but suggests that the mole fraction profile measured at 11.1 eV contains a substantial contribution from ethenol.

In some cases the difference in ionization energies of two species with a given  $m/z$  ratio is so small that PIE curves do not show distinguishing features. Ion signals for  $m/z = 29$  have not been resolved into contributions from HCO and C<sub>2</sub>H<sub>5</sub>, which have nominal ionization energies of  $8.12 \pm 0.04$  eV<sup>35</sup> and  $8.117 \pm 0.008$  eV,<sup>35</sup> respectively.

The mole fraction profiles measured for  $m/z = 56$  at 10.4 eV for ethyl formate and at 9.7 and 10.4 eV for methyl acetate are likely to represent superpositions of contributions from butene isomers, methyl ketene and other isomers. A successful approach for the identification of some of the different isomers at mass 56 is presented elsewhere,<sup>38</sup> but was not attempted in this experiment. No mole fraction profiles were obtainable for C<sub>2</sub>H<sub>6</sub> because of the presence of strong interferences from formaldehyde at  $m/z = 30$ .<sup>27,29</sup>

**2.2. Data Analysis. 2.2.1. Major Species.** Data reduction procedures required for determinations of mole fractions for the major species (the fuel, O<sub>2</sub>, Ar, CO, CO<sub>2</sub>, H<sub>2</sub>O, and H<sub>2</sub>) from photoion signals are described elsewhere.<sup>27,29,30</sup> In the present experiments, ion signals from methyl acetate or ethyl formate at 11.1 eV, O<sub>2</sub> at 12.3 eV, CO and CO<sub>2</sub> at 14.1 eV, H<sub>2</sub>O at 13.2 eV, and H<sub>2</sub> at 16.6 eV are recorded for all burner–cone

separations extending to approximately 30 mm from the burner. The H<sub>2</sub>O signals are corrected for background contributions by subtraction of the  $m/z = 18$  signal extrapolated to the burner surface. As an approximation, this correction is one-half of the  $m/z = 18$  signal recorded with the smallest practical separation (1.2 mm) between the sampling cone and the surface. The usefulness of this approximation was supported by recording the  $m/z = 18$  signals, found to be nearly constant for all burner positions, associated with background H<sub>2</sub>O for D<sub>2</sub>/O<sub>2</sub>/Ar flames. The CO signals are corrected for contributions from the C<sub>2</sub>H<sub>4</sub> profile. Corrections are also made for a small O<sub>2</sub> signal at 30 mm, attributable to background O<sub>2</sub> from residual air in the mass spectrometer chamber.

**2.2.1.1. Post-Flame Zone.** The first step in the conversion of the measured ion signals yields major species mole fractions in the post-flame region far (ca. 30 mm) from the burner. In separate experiments, the ratio of signals for CO and CO<sub>2</sub> at 14.1 eV is measured for a cold flow of a calibration gas mixture containing equal parts of CO and CO<sub>2</sub>. This ratio is used with the ratio of signals measured at 30 mm in the post flame zone to compute the ratio of CO to CO<sub>2</sub> mole fractions at this flame position. This mole fraction ratio and C, O, and H atom balances are then used to determine the mole fractions of Ar, CO, CO<sub>2</sub>, H<sub>2</sub>O, and H<sub>2</sub> at 30 mm, subject to the approximation that the sum of mole fractions for these species is unity. These are the only species with significant ion signals at this flame position; signals from O, OH, and H are too small for quantitative analysis. Neglect of these radicals produces a potential error of about 5% in the summation, based on experimental and modeling results for oxygenated hydrocarbon flames.<sup>29</sup>

**2.2.1.2. Mole Fraction Profiles.** At this point two different approaches employed for the calculation of the mole fraction profiles for the major species throughout the flames yield almost indistinguishable results. Both of these methods provide a link between recorded ion signals and mole fractions for a given flame species. This link is expressed with the following relationship:<sup>27</sup>

$$S_i = x_i \sigma_i(E) D(M_i) \Phi c \text{FKT} \quad (1)$$

Here  $S_i$  is the ion signal (integrated ion count recorded for a flame species  $i$ );  $x_i$  is the species mole fraction;  $\sigma_i(E)$  is the photoionization cross section at the photon energy  $E$ ;  $D(M_i)$  is the mass discrimination factor<sup>26,27</sup> for species  $i$ ;  $\Phi$  is the photon current;  $c$  is an instrument-dependent constant of proportionality, and FKT is an instrumental sampling function that relates the molecular beam molar density at the ionization region to the flame pressure and local temperature.

Under identical instrumental conditions, signals at a defined flame position can be expressed relative to a reference species R with the relationship:<sup>27</sup>

$$\frac{S_i}{S_R} = \frac{x_i \sigma_i(E) D(M_i)}{x_R \sigma_R(E) D(M_R)} = \frac{x_i}{x_R} k_i \quad (2)$$

In the first approach, the calibration factors  $k_i$  for a given species with respect to argon as the reference species are used in the expression

$$x_{\text{Ar}} = 1 - x_{\text{Ar}} \sum \frac{S_i}{S_{\text{Ar}} k_i} \quad (3)$$

to yield the local argon mole fraction at a given flame position, for which the ratios of ion signals  $S_i/S_{\text{Ar}}$  are measured for the major species (CO, CO<sub>2</sub>, H<sub>2</sub>, H<sub>2</sub>O, O<sub>2</sub>, and fuel). The calibration

**TABLE 2: Photon Energies  $E$ , Peak Mole Fractions  $x_{\text{max}}$  and Peak Positions (DFB)<sup>a</sup>**

	methyl acetate			ethyl formate		
	$E$ [eV]	$x_{\text{max}}$	DFB [mm]	IE [eV]	$x_{\text{max}}$	DFB [mm]
Ar <sup>b</sup>	16.6	1.4E-01	30.3	16.6	1.4E-01	30.3
fuel <sup>b</sup>	10.4	2.5E-01	0.0	11.1	2.5E-01	0.0
O <sub>2</sub> <sup>b</sup>	12.3	4.9E-01	0.0	12.3	4.9E-01	0.0
H <sub>2</sub> <sup>b</sup>	16.6	1.4E-01	30.3	16.6	1.4E-01	30.3
H <sub>2</sub> O <sup>b</sup>	13.2	2.9E-01	30.3	13.2	2.9E-01	30.3
CO <sub>2</sub> <sup>b</sup>	14.1	1.1E-01	30.3	14.1	1.1E-01	30.3
CO <sup>b</sup>	14.1	3.1E-01	30.3	14.1	3.1E-01	30.3
CH <sub>3</sub>	10.4	5.2E-03	4.3	10.4	1.7E-03	3.8
CH <sub>4</sub>	13.2	1.2E-02	4.3	13.2	4.2E-03	3.3
HCO	10.4	2.1E-04	4.3	10.4	3.7E-04	2.8
CH <sub>2</sub> O	11.1	1.6E-02	3.3	11.1	4.4E-03	2.8
CH <sub>3</sub> OH	11.1	3.8E-03	4.3	11.1	5.2E-04	1.8
C <sub>2</sub> H <sub>2</sub>	12.3	8.6E-03	5.3	12.3	3.2E-02	4.3
C <sub>2</sub> H <sub>4</sub>	11.1	7.8E-03	4.3	11.1	7.0E-02	3.3
H <sub>2</sub> CCO	10.4	6.8E-03	4.3	10.4	1.9E-03	3.8
CH <sub>3</sub> CO	9.6	2.0E-04	4.3	10.4	7.5E-05	2.8
CH <sub>3</sub> CHO	10.4	2.7E-04	3.8	10.4	3.9E-03	2.8
(CH <sub>3</sub> ) <sub>2</sub> O	10.4	5.6E-05	3.3	10.4	4.5E-05	2.3
CH <sub>3</sub> COOH	11.1	8.0E-04	3.8	11.1	4.2E-05	2.8
C <sub>3</sub> H <sub>3</sub>	9.6	7.0E-05	4.8	10.4	1.2E-04	4.3
C <sub>3</sub> H <sub>4</sub>	10.4	7.3E-05	4.8	10.4	9.6E-05	4.3
$m/z$ 56	9.6	2.6E-05	3.8	10.4	5.0E-05	3.3
(CH <sub>3</sub> ) <sub>2</sub> CO	10.4	1.3E-04	3.3	10.4	6.0E-05	2.8
C <sub>4</sub> H <sub>2</sub>	10.4	8.6E-05	5.3	10.4	3.4E-04	5.3
C <sub>4</sub> H <sub>4</sub>	9.6	4.1E-05	4.8	10.4	1.1E-04	4.3
C <sub>4</sub> H <sub>6</sub>	9.6	2.8E-05	3.8	10.4	1.1E-04	3.3
cyclo-C <sub>5</sub> H <sub>6</sub>	10.4	1.0E-05	3.3	10.4	9.7E-06	4.3
C <sub>6</sub> H <sub>6</sub>	10.4	<1.0E-06	ND	10.4	4.0E-06	3.3

<sup>a</sup>ND: not detected. DFB: distance from burner. <sup>b</sup>Initial or post flame values.

factors can in principle be calculated for each of the species when the photoionization cross sections and mass discrimination factors are known. We instead apply eq 2 at 30 mm in the post flame, where the mole fractions of CO, CO<sub>2</sub>, H<sub>2</sub> and H<sub>2</sub>O are known (cf. section 2.2.1.1). Calibration factors for O<sub>2</sub> and the fuel are derived from their respective signals and initial mole fractions at the burner face. Finally, in this approach, knowledge of the calibration factors  $k_i$  enables calculation of the argon mole fraction at every burner position with eq 3. Mole fraction profiles for the remaining major species are calculated with eq 2.

In the second approach, measurements of the argon ion signal at 16.6 eV throughout the flame yield an empirical instrumental sampling function FKT, according to the procedure of ref 27. Mole fraction profiles for all major species are then calculated as described elsewhere.<sup>27,29</sup>

Major species mole fractions derived with both approaches differ by less than 10% at all flame positions. We estimate an uncertainty of  $\pm 15$ –20% in these major species mole fractions for either method. The results displayed in parts a and b of Figure 2 are determined with the first approach.

**2.2.2. Intermediate Species.** Here again two independent approaches are followed for data analysis. In the first approach, intermediate species mole fractions are derived directly from eq 1. The product  $c \times \text{FKT}$  is found with measurements, at each position in the flame, of the argon ion signal at 16.6 eV and from knowledge of the argon mole fractions (cf. section 2.2.1.2). Application of eq 1 requires corrections for any changes in experimental parameters for measurements for other species at other energies. This direct procedure involves a minimum number of cross sections and thus potentially reduces the absolute error of the minor species mole fractions. Values for  $\sigma_i(E)$  and  $D(M_i)$  used in the data analysis are given in Table 1.

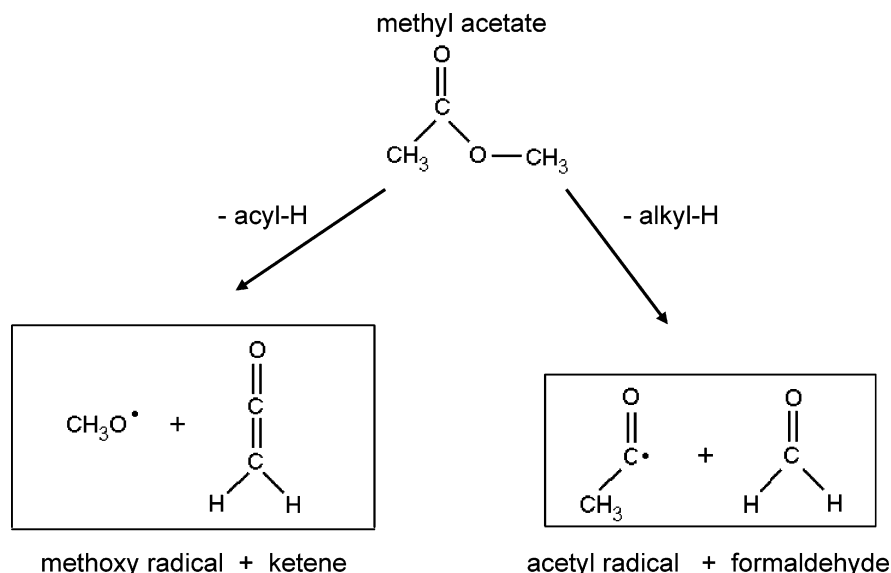


**Figure 3.** Pathways for destruction of methyl acetate by H atom abstraction from the acyl ( $\text{CH}_3$ ) and alkoxy ( $\text{OCH}_3$ ) functional groups of methyl acetate.

In the second approach, mole fractions for intermediate species are determined using eq 2 to reference the mole fraction for species  $i$  to that of a second reference species of known mole fraction. The mole fraction profiles for  $\text{CH}_4$  and  $\text{C}_2\text{H}_2$  are derived from that of  $\text{H}_2\text{O}$  at 13.2 eV. The  $\text{C}_2\text{H}_4$  mole fraction profile requires measurements of ion signals from  $\text{C}_2\text{H}_2$  and  $\text{C}_2\text{H}_4$  at 11.5 eV, an energy chosen to avoid fragment  $\text{C}_2\text{H}_4^+$  ions from  $\text{C}_2\text{H}_6$  at higher photon energies. Mole fractions for  $\text{CH}_2\text{O}$ ,  $\text{C}_4\text{H}_2$ , and  $\text{C}_4\text{H}_4$  are next derived from  $\text{C}_2\text{H}_4$  with ion signals at 11.5 and/or 12.3 eV and checked for consistency by comparing results for pairs of molecules at 11.1, 11.5, or 12.3 eV. One or more of these four molecules served as references for the remaining species with measurements at 11.1, 10.4, or 9.65 eV for methyl acetate and 11.1, 10.4, or 9.0 eV for ethyl formate. These results were also checked, where possible, using redundant determinations, pairing a given species with more than one reference species.

The intermediate species mole fractions presented here were all determined with the first approach except for the acetic acid and acetyl radical profiles. The peak mole fractions for these species determined with both methods are in fair agreement ( $\pm 30\%$ ), but the profiles obtained with the second method exhibit better signal-to-noise ratio and are therefore more reliable. No clear trends were observed in the discrepancies between calculations performed with the alternate methods; these differences are typically  $\pm 20\%$  for most intermediate species (ranging from  $\pm 5\%$  for  $\text{CH}_3$  in the ethyl formate flame to  $\pm 30\%$  for  $\text{CH}_2\text{O}$  in the methyl acetate flame).

The accuracy of mole fractions for stable intermediates with known photoionization cross sections is estimated to be  $\pm 30\text{--}40\%$ , while radical species and minor stable intermediates with estimated photoionization cross sections are uncertain by factors of 2–4. However, because the apparatus and data reduction procedures are the same for both flames, relative comparisons of mole fractions between flames have probable uncertainties of  $\pm 15\%$  for most intermediates, except for those with the lowest mole fractions (ca. 10 ppm) which exhibit uncertainties of  $\pm 30\%$ .

### 3. Results

Species mole fractions were measured and compared for premixed  $\text{CH}_3(\text{CO})\text{OCH}_3/\text{O}_2/\text{Ar}$  and  $\text{H}(\text{CO})\text{OC}_2\text{H}_5/\text{O}_2/\text{Ar}$  flames

of identical equivalence ratio. Maximum mole fraction values for a number of observed species and their respective positions with respect to the burner surface are reported in Table 2. The temperature profiles and mole fraction profiles for major species,  $\text{O}_2$ ,  $\text{CO}$ ,  $\text{CO}_2$ ,  $\text{H}_2\text{O}$ ,  $\text{H}_2$ , Ar, and fuels, were found to be quite similar for the isomeric fuels, as illustrated in Figure 2, parts a and b. This observation supports the suitability of the isomeric fuel approach to the elucidation of the fuel-specific reaction pathways.

**3.1. Fuel-Specific Destruction Pathways.** Fuel-specific destruction pathways for methyl acetate and ethyl formate are illustrated in Figures 3 and 4. The initial destruction of both esters occurs by H-abstraction under these flame conditions. An H atom may be abstracted from either the acyl or alkoxy group of each fuel.<sup>9</sup>

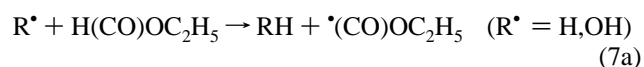
**3.1.1. Methyl Acetate.** For methyl acetate, abstraction of an acyl hydrogen followed by  $\beta$ -scission of the  $\cdot\text{CH}_2(\text{CO})\text{OCH}_3$  intermediate yields the methoxy radical and ketene:



H atom abstraction from the methoxy group of methyl acetate forms the acetyl radical and formaldehyde by  $\beta$ -scission of  $\text{CH}_3(\text{CO})\text{OCH}_2^\bullet$ :



**3.1.2. Ethyl Formate.** For ethyl formate, acyl H-abstraction yields the ethoxy radical and carbon monoxide following  $\alpha$ -scission of the  $\cdot(\text{CO})\text{OC}_2\text{H}_5$  intermediate:



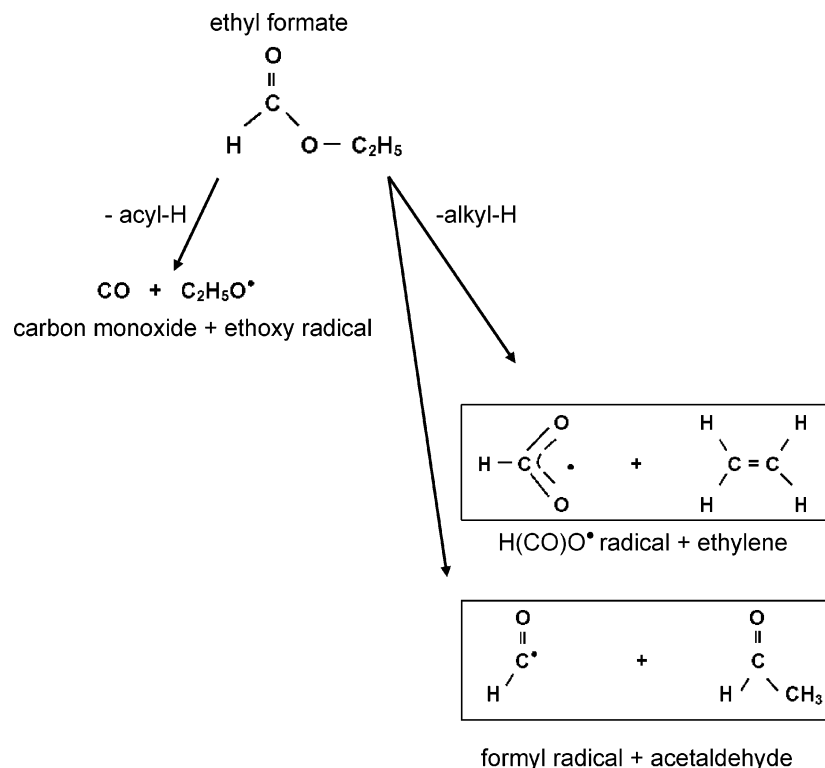
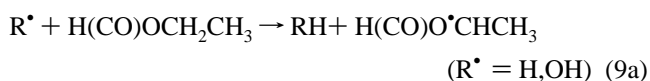


**Figure 4.** Fuel-specific destruction pathways for H atom abstractions from ethyl formate.

Abstraction of a primary hydrogen from the ethoxy group of ethyl formate yields the H(CO)O<sup>•</sup> radical and ethylene, while abstraction of a secondary hydrogen gives the formyl radical and acetaldehyde:



While the major species profiles for both flames (cf. Figure 2, parts a and b) show good agreement for the two flames, pronounced fuel-specific effects are evident in the mole fraction profiles of intermediate species.

**3.2. Discussion of Mole Fraction Profiles.** The mole fractions for the key reaction intermediates CH<sub>2</sub>O, C<sub>2</sub>H<sub>4</sub>, C<sub>2</sub>H<sub>2</sub>, CH<sub>3</sub>CHO, CH<sub>4</sub>, and CH<sub>3</sub> in the ethyl formate and methyl acetate flames are displayed in Figure 5. The concentrations of ethylene and acetylene are 9 and 4 times larger for the ethyl formate flame, respectively. The presence of the ethyl group suggests that ethyl formate may decompose into smaller species with carbon-carbon bonds. In the ethyl formate flame this would provide a direct pathway to C<sub>2</sub>H<sub>4</sub> (e.g., reaction 8, parts a and b) and C<sub>2</sub>H<sub>2</sub> which could in turn be formed by dehydrogenation of C<sub>2</sub>H<sub>4</sub>. Other pathways to C<sub>2</sub>H<sub>4</sub> include formation from C<sub>2</sub>H<sub>6</sub> resulting from the association of methyl radicals and the CH<sub>3</sub> + CH<sub>2</sub> ⇌ C<sub>2</sub>H<sub>4</sub> + H reaction. Such less direct pathways are expected to be most important in the methyl acetate flame with its higher CH<sub>3</sub> concentration. The relatively smaller concentra-

tions of C<sub>2</sub>H<sub>4</sub> and C<sub>2</sub>H<sub>2</sub> in the methyl acetate flame suggest the importance of the fuel-specific destruction of ethyl formate by reaction 8, parts a and b. The β-scission of the fuel radical (reaction 8b) yielding CO<sub>2</sub> as a decomposition product may account for the observed steeper rise of the CO<sub>2</sub> profile, which is noticeable up to a distance of more than 5 mm.

Substantial mole fractions of acetaldehyde are seen in the ethyl formate flame as expected from the reaction 9, parts a and b. In contrast, the acetaldehyde concentration in the methyl acetate flame is 14 times smaller. The influence of alkyl side chains is evident in the methyl and methane concentrations, which are approximately three times larger for the methyl acetate flame. The concentration of formaldehyde is four times greater for the methyl acetate flame, as suggested from reaction 6, parts a and b.

Fuel-specific differences between the flames are also seen in several minor intermediates, as shown in Figure 6. Ketene, a direct fuel destruction product of methyl acetate (cf. reaction 5, parts a and b), is more prominent in the methyl acetate flame with four times higher concentration. On the other hand, the HCO/C<sub>2</sub>H<sub>5</sub> concentration is higher in the ethyl formate flame, consistent with the formation of HCO by reaction 9, parts a and b. The acetyl radical (cf. reaction 6, parts a and b) and the hydrolysis products methanol and acetic acid are prominent intermediates in the methyl acetate flame; the products of the hydrolysis of ethyl formate (ethanol and formic acid), however, are not quantified because of an apparent interference of undetermined origin at *m/z* = 46. Therefore, only methanol, acetic acid, and acetyl radical are displayed in Figure 6. As expected, the concentrations of these three species are considerably lower in the ethyl formate flame.

Important C<sub>3</sub> and C<sub>4</sub> hydrocarbons are shown in Figures 7 and 8. C<sub>3</sub>H<sub>3</sub> and C<sub>3</sub>H<sub>4</sub> (predominately propyne, cf. Figure 1) are observed at similar concentrations in both flames, while diacetylene, C<sub>4</sub>H<sub>2</sub>, vinylacetylene, C<sub>4</sub>H<sub>4</sub>, and 1,3-butadiene are

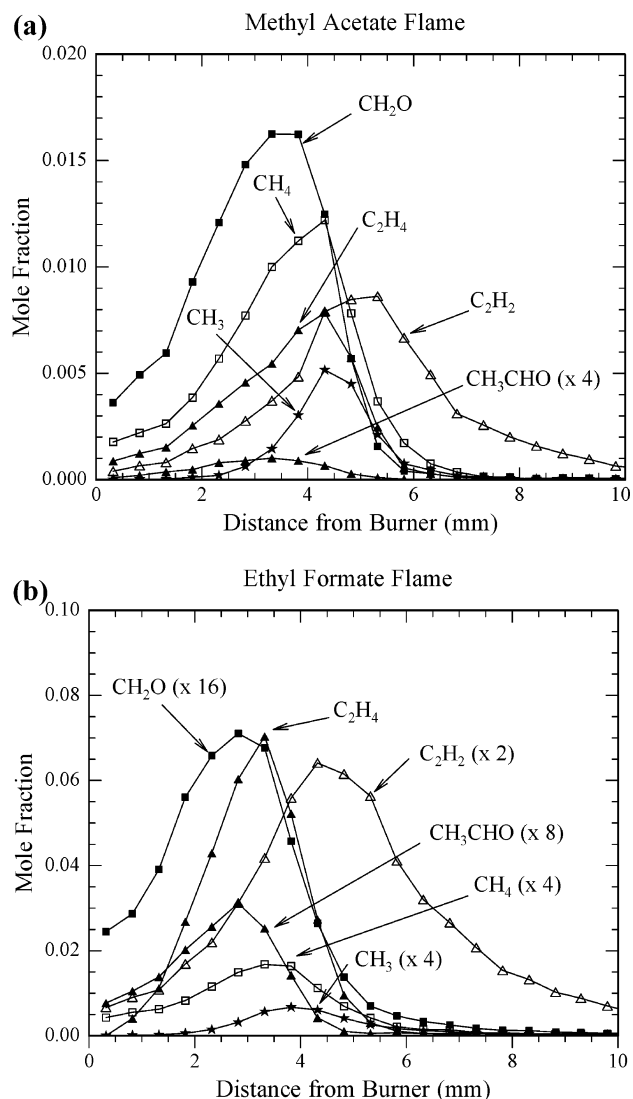


**Figure 5.** Comparison of mole fraction profiles for key intermediate species in the methyl acetate (a) and ethyl formate (b) flames.

more abundant in the ethyl formate flame by factors of 4, 3, and 4, respectively. This difference is consistent with the expectation that flames with high concentrations of acetylene provide easy access to  $C_4$  hydrocarbons. Both flames exhibit higher-mass species as shown in Figure 8, including the oxygenates dimethyl ether and acetone as well as hydrocarbon intermediates such as cyclopentadiene.

Benzene reaches higher levels in the ethyl formate flame. Propargyl, propyne, acetylene, diacetylene, and vinylacetylene are all thought to be related to the formation of benzene, the first step in the formation of polycyclic aromatics. The  $m/z = 78$  signal for the ethyl formate flame is detected above the background at 10.4 eV with a signal-to-background ratio of 3, while no  $m/z = 78$  signal above background was seen for the methyl acetate flame. The estimated benzene mole fraction in the ethyl formate flame is 4 ppm, accurate to about a factor of 2. This level is comparable to benzene concentrations seen in fuel-rich ( $\Phi = 2.5$ ) ethanol flames (7 ppm)<sup>39</sup> but about 2 orders of magnitude lower than those in fuel-rich ( $\Phi = 1.8\text{--}2.3$ )  $C_3$ -hydrocarbon flames, e.g., propane<sup>27</sup> and propene<sup>30</sup> and allene/propyne.<sup>40</sup>  $C_3H_3$ ,  $C_4H_2$ , and  $C_4H_4$  are also seen in ethanol flames<sup>39</sup> at mole fractions comparable to those reported here for ethyl formate and methyl acetate and are significantly lower compared to mole fractions in flames of hydrocarbon fuels.

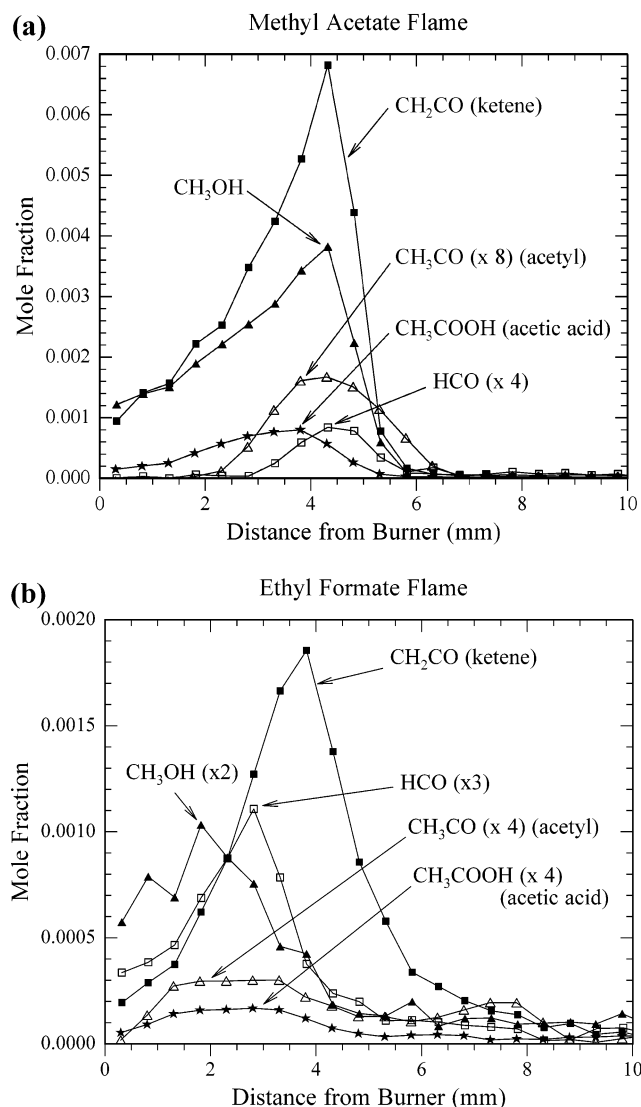


**Figure 6.** Comparison of selected oxygenated intermediate species in the methyl acetate (a) and ethyl formate (b) flames.

Taken together, these findings are consistent with the observation that biodiesel tends to reduce soot formation.<sup>6</sup> Propargyl self-combination<sup>41,42</sup> has been identified in many flames as the main source of benzene and lower  $C_3H_3$  concentrations relative to hydrocarbon flames will form benzene more slowly. The observed maximum  $C_3H_3$  concentration in the ethyl formate flame is about a factor of 2 larger than that of the methyl acetate flame (see Table 2 and Figure 7). This suggests a peak benzene concentration of about 1 ppm for methyl acetate, four times smaller than that estimated for the ethyl formate flame and just below the detection limit. The differing benzene yield from the two ester flames may also, however, suggest that  $C_2H_2$  and/or  $C_4H_x$  chemistry may contribute to benzene formation. There is a controversial history of possible  $C_2H_2 + C_4H_x$  routes in the literature.<sup>28,43,44</sup> The higher yield of  $C_6H_6$  for ethyl formate is an intriguing subject for further study in future work. Note that the processes leading to soot in an engine include additional complex interactions, and depend on the physical as well as chemical properties of the fuel.<sup>6,21,45,46</sup> The present results for the simplest esters suggest that the ester function may significantly influence the formation of benzene and soot even for practical biodiesel fuels with long hydrocarbon chains.

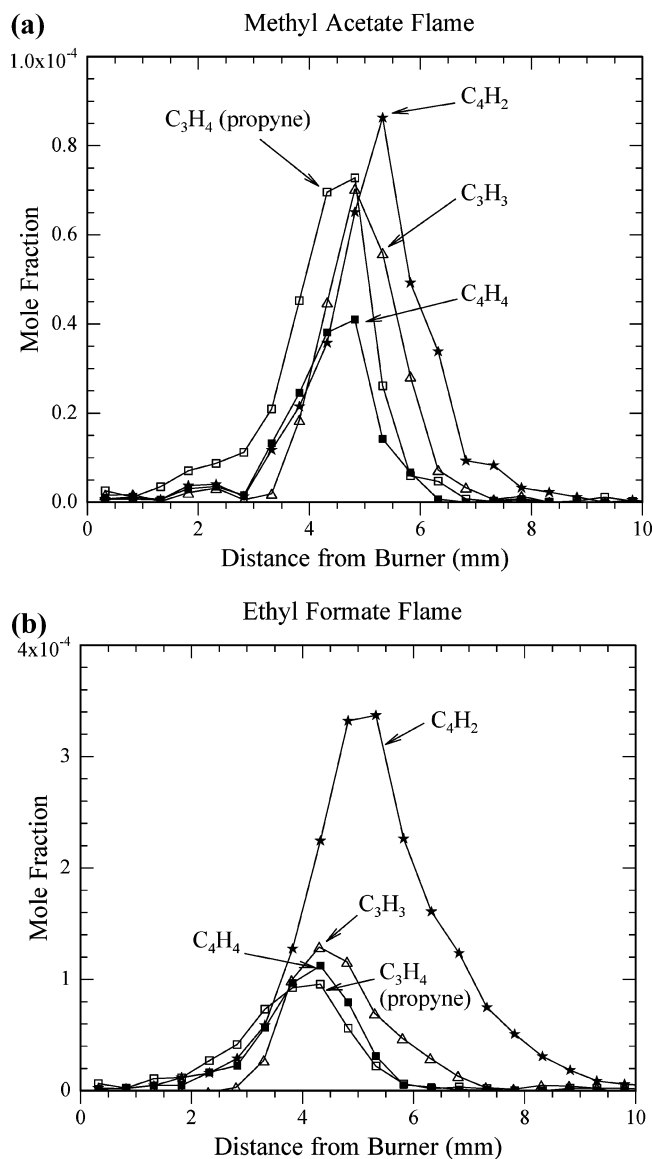


**Figure 7.** Comparison of selected C<sub>3</sub> and C<sub>4</sub> precursors to the formation of benzene for the methyl acetate (a) and ethyl formate (b) flames.

#### 4. Conclusions and Combustion-Chemistry Implications

The methyl acetate and ethyl formate structural isomers were selected as model compounds to investigate the combustion chemistry of methyl and ethyl esters, typical constituents of biodiesel fuels. Quantitative comparisons of intermediate species compositions reveal differences directly associated with structurally dependent reaction pathways initiated by H atom abstractions.

To analyze important reaction sequences involved in the combustion of these two isomeric ester flames, absolute mole fraction profiles are presented for 27 species in low-pressure laminar premixed flat flames under identical flame conditions. Isomer-selective photoionization, using monochromated synchrotron radiation coupled with molecular beam mass spectrometry, provides the first quantitative observations of the composition of reaction intermediates for laminar premixed alkyl ester flames.

With regard to the formation of the regulated pollutants formaldehyde and acetaldehyde, our results indicate that H-abstraction from the methoxy group of the methyl ester (reaction 6, parts a and b) leads to preferential formation of formaldehyde, while H-abstraction from the ethoxy group of the ethyl ester

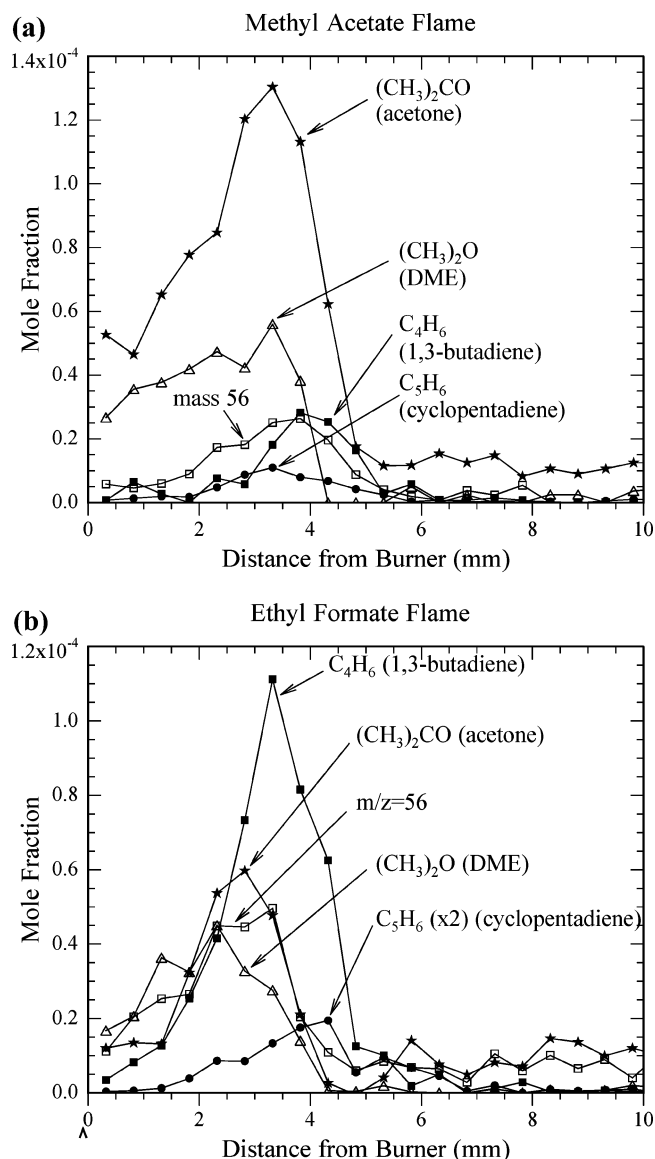


**Figure 8.** Mole fraction profiles for selected higher mass intermediates.

(reaction 9, parts a and b) leads to substantially greater concentrations of acetaldehyde for the ethyl formate flame. Our preliminary measurements for methyl formate and ethyl acetate flames lead to similar conclusions. Detailed combustion modeling is needed to assess the importance of these direct decompositions relative to reactions involving the hydrolysis products, methanol and ethanol, of methyl and ethyl esters, respectively. Such modeling may ultimately yield quantitative descriptions of the prevalence of formaldehyde (acetaldehyde) emissions predicted for biodiesel formulations containing methyl esters (ethyl esters).

Lower C<sub>3</sub>H<sub>3</sub> concentrations compared to hydrocarbon flames accounts for the lower benzene formation, while the ethyl group is responsible for the formation of significantly larger concentrations of C<sub>2</sub> and C<sub>4</sub> species for ethyl formate than from methyl acetate. Direct formation of C<sub>2</sub>H<sub>4</sub> by H-abstraction of a primary hydrogen from the ethoxy group of ethyl formate, followed by  $\beta$ -scission, is identified as a possible source for this enhancement in C<sub>2</sub> and C<sub>4</sub> species. Kinetic modeling is needed to establish the relative contribution of this process compared with the dehydrogenation sequence C<sub>2</sub>H<sub>6</sub>  $\rightarrow$  C<sub>2</sub>H<sub>5</sub> + H  $\rightarrow$  C<sub>2</sub>H<sub>4</sub> + H + H, following the association of methyl radicals, and the CH<sub>3</sub> + CH<sub>2</sub>  $\rightleftharpoons$  C<sub>2</sub>H<sub>4</sub> + H reaction, both expected to be more important

for the methyl acetate flame, which has a larger concentration of CH<sub>3</sub> radicals. Although the growth of soot via the “even carbon” precursors such as C<sub>4</sub>H<sub>5</sub> and C<sub>4</sub>H<sub>3</sub><sup>43,44</sup> is thought to be substantially less important than the “odd carbon” route centered on the propargyl radical,<sup>41,42</sup> the increased C<sub>2</sub> and C<sub>4</sub> intermediates in the ethyl ester flame may have implications for the progress of molecular-weight growth and soot formation in ester combustion.

These and similar measurements on other alkyl ester flames, coupled with kinetic modeling, are needed to address the challenge of the quantitative description of the key reaction mechanisms responsible for observed reductions in unburned hydrocarbons, polycyclic aromatic hydrocarbons, carbon monoxide, and particulate emissions when biodiesel is used as a partial or complete replacement for conventional petroleum diesel fuels. Comparison of the methyl vs ethyl ester combustion chemistry considered here is relevant in the more general context of the combustion of practical biodiesel compounds, which often exhibit analogous structural features.

**Acknowledgment.** The authors thank Paul Fugazzi, Michael Jimenez-Cruz, Musahid Ahmed, and John Bozek for expert technical assistance at the Advanced Light Source and Linda-Christin Salameh for assistance with measurements at the University of Bielefeld. They are grateful to Craig Taatjes for helpful discussions. This work is supported by the Division of Chemical Sciences, Geosciences, and Biosciences, Office of Basic Energy Sciences, U.S. Department of Energy (USDOE), in part under grants DE-FG02-01ER15180 (T.A.C, J.W.), DE-FG02-91ER14192 (P.R.W.); by the Chemical Sciences Division, U.S. Army Research Office (T.A.C, J.W.); and by the Deutsche Forschungsgemeinschaft KO 1363/18-3 (P.O., U.S., T.K., K.K.-H.) Sandia is a multiprogram laboratory operated by Sandia Corporation, a Lockheed Martin Company, for the National Nuclear Security Administration under contract DE-AC04-94-AL85000. The Advanced Light Source is supported by the Director, Office of Science, Office of Basic Energy Sciences, Materials Sciences Division, of the USDOE under Contract No. DE-AC02-05CH11231 at Lawrence Berkeley National Laboratory.

## References and Notes

- Ragauskas, A. J.; Williams, C. K.; Davison, B. H.; Britovsek, G.; Cairney, J.; Eckert, C. A.; Frederick, Jr., W. J.; Hallet, J. P.; Leak, D. J.; Liotta, C. L.; Mielenz, J. R.; Murphy, R.; Templer, R.; Tschaplinski, T. *Science* **2006**, *311*, 484.
- Venkataraman, C.; Habib, G.; Eiguren-Fernandez, A.; Miguel, A. H.; Friedlander, S. K. *Science* **2005**, *307*, 1454.
- Farrell, A. E.; Plevin, R. J.; Turner, B. T.; Jones, A. D.; O'Hare, M.; Kammen, D. M. *Science* **2006**, *311*, 506.
- Singh, B. H.; Kanakidou, M.; Crutzen, P. J.; Jacob, D. J. *Nature (London)* **1995**, *378*, 50.
- Westbrook, C. K.; Pitz, W. J.; Curran, H. J. *J. Phys. Chem. A* **2006**, *110*, 6912.
- Graboski, M. S.; McCormick, R. L. *Prog. Energy Combust. Sci.* **1998**, *24*, 125.
- Demirbaş, A. *Prog. Energy Combust. Sci.* **2007**, *33*, 1.
- Crookes, R. J. *Biomass Bioenerg.* **2006**, *30*, 461.
- Hoare, D. E.; Kamil, M. *Combust. Flame* **1970**, *15*, 61.
- Gil'burd, M. M.; Moin, F. B. *J. Catal.* **1968**, *10*, 95.
- Sulzmann, K. G. P.; Baxter, D. E.; Khazra, M.; Lund, T. S. *J. Phys. Chem.* **1985**, *89*, 3561.
- Dagaut, P.; Smoucovit, N.; Cathonnet, M. *Combust. Sci. Technol.* **1997**, *127*, 275.
- Christensen, L. K.; Ball, J. C.; Wallington, T. J. *J. Phys. Chem. A* **2000**, *104*, 345.
- Wallington, T. J.; Hurlley, M. D.; Maurer, T.; Barnes, I.; Becker, K. H.; Tyndall, G. S.; Orlando, J. J.; Pimentel, A. S.; Bilde, M. *J. Phys. Chem. A* **2001**, *105*, 5146.
- Fisher, E. M.; Pitz, W. J.; Curran, H. J.; Westbrook, C. K. *Proc. Combust. Inst.* **2000**, *28*, 1579.
- Gasnot, L.; Decottignies, V.; Pauwels, J. F. *Fuel* **2005**, *84*, 505.
- Sarathy, S. M.; Gail, S.; Syed, S. A.; Thomson, M. J.; Dagaut, P. *Proc. Combust. Inst.* **2007**, *31*, 1015.
- Gail, S.; Thomson, M. J.; Sarathy, S. M.; Syed, S. A.; Dagaut, P.; Diévert, P.; Marchese, A. J.; Dryer, F. L. *Proc. Combust. Inst.* **2007**, *31*, 305.
- Dagaut, P.; Gail, S.; Sahasrabudhe, M. *Proc. Combust. Inst.* **2007**, *31*, 2955.
- Pouloupoulos, S. G.; Philippopoulos, C. J. *J. Eng. Gas Turbines Power-Trans. ASME* **2003**, *125*, 344.
- Lotero, E.; Liu, Y.; Lopez, D. E.; Suwannakarn, K.; Bruce, D. A.; Goodwin, J. G., Jr. *Ind. Eng. Chem. Res.* **2005**, *44*, 5353.
- Parsons, B. I.; Danby, C. J. *J. Chem. Soc.* **1956**, 1795.
- Parsons, B. I.; Hinshelwood, C. J. *J. Chem. Soc.* **1956**, 1799.
- Parsons, B. I. *J. Chem. Soc.* **1956**, 1804.
- Cool, T. A.; Nakajima, K.; Mostefaoui, T. A.; Qi, F.; McIlroy, A.; Westmoreland, P. R.; Law, M. E.; Poisson, L.; Peterka, D. S.; Ahmed, M. *J. Chem. Phys.* **2003**, *119*, 8356.
- Cool, T. A.; McIlroy, A.; Qi, F.; Westmoreland, P. R.; Poisson, L.; Peterka, D. S.; Ahmed, M. *Rev. Sci. Instrum.* **2005**, *76*, Art. No. 094102.
- Cool, T. A.; Nakajima, K.; Taatjes, C. A.; McIlroy, A.; Westmoreland, P. R.; Law, M. E.; Morel, A. *Proc. Combust. Inst.* **2005**, *30*, 1681.
- Hansen, N.; Klippenstein, S. J.; Taatjes, C. A.; Miller, J. A.; Wang, J.; Cool, T. A.; Yang, B.; Yang, R.; Wei, L.; Huang, C.; Wang, J.; Qi, F.; Law, M. E.; Westmoreland, P. R. *J. Phys. Chem. A* **2006**, *110*, 3670.
- Cool, T. A.; Wang, J.; Hansen, N.; Westmoreland, P. R.; Dryer, F. L.; Zhao, Z.; Kazakov, A.; Kasper, T.; Kohse-Höinghaus, K. *Proc. Combust. Inst.* **2007**, *31*, 285.
- Kohse-Höinghaus, K.; Osswald, P.; Struckmeier, U.; Kasper, T.; Hansen, N.; Taatjes, C. A.; Wang, J.; Cool, T. A.; Gon, S.; Westmoreland, P. R. *Proc. Combust. Inst.* **2007**, *31*, 1119.
- Wiley, W. C.; McLaren, J. H. *Rev. Sci. Instrum.* **1955**, *26*, 1150.
- Hartlieb, A. T.; Atakan, B.; Kohse-Höinghaus, K. *Appl. Phys. B: Laser Opt.* **2000**, *70*, 435.
- Biordi, J. C.; Lazzara, C. P.; Papp, J. F. *Combust. Flame* **1974**, *23*, 73.
- Cattolica, R. J.; Yoon, S.; Knuth, E. L. *Combust. Sci. Technol.* **1982**, *28*, 225.
- Linstrom, P. J.; Mallard, W. G., Eds. *NIST Chemistry WebBook, NIST Standard Reference Database Number 69*; National Institute of Standards and Technology: Gaithersburg, MD, 2003; <http://webbook.nist.gov>.
- Cool, T. A.; Wang, J.; Nakajima, K.; Taatjes, C. A.; McIlroy, A. *Int. J. Mass Spectrom.* **2005**, *247*, 18.
- Taatjes, C. A.; Hansen, N.; McIlroy, A.; Miller, J. A.; Senosiain, J. P.; Klippenstein, S. J.; Qi, F.; Sheng, L.; Zhang, Y.; Cool, T. A.; Wang, J.; Westmoreland, P. R.; Law, M. E.; Kasper, T.; Kohse-Höinghaus, K. *Science* **2005**, *308*, 1887.
- Hansen, N.; Kasper, T.; Klippenstein, S. J.; Westmoreland, P. R.; Law, M. E.; Taatjes, C. A.; Kohse-Höinghaus, K.; Wang, J.; Cool, T. A. *J. Phys. Chem. A*, in press (2007).
- Kasper, T. S.; Osswald, P.; Kamphus, M.; Kohse-Höinghaus, K. *Combust. Flame*, in press (2006).
- Hansen, N.; Miller, J. A.; Taatjes, C. A.; Wang, J.; Cool, T. A.; Law, M. E.; Westmoreland, P. R. *Proc. Combust. Inst.* **2007**, *31*, 1157.
- Miller, J. A.; Melius, C. F. *Combust. Flame* **1992**, *91*, 21.
- Miller, J. A.; Klippenstein, S. J. *J. Phys. Chem. A* **2003**, *107*, 7783.
- Westmoreland, P. R.; Dean, A. M.; Howard, J. B.; Longwell, J. P. *J. Phys. Chem.* **1989**, *93*, 8171.
- Wang, H.; Frenklach, M. *Combust. Flame* **1997**, *110*, 173.
- U. S. EPA A comprehensive analysis of biodiesel impacts on exhaust emissions. U.S. EPA document EPA-420-P-02-001, Office of Transportation and Air Quality: Ann Arbor, MI (2002).
- Mueller, C. I.; Pitz, W. J.; Pickett, L. M.; Martin, G. C.; Siebers, D. L.; Westbrook, C. K. SAE paper-2003-01-1797 (JSAE 20020193), 2003.